

Multifunctional Separator Coatings for High-Performance Lithium–Sulfur Batteries

Mun Sek Kim, Lin Ma, Snehashis Choudhury, and Lynden A. Archer*

Electrochemical energy storage systems that are cost-effective, safe, environmentally friendly, and possess long cycle/shelf-life are needed in multiple fields of technology, including transportation, portable devices, robotics, and power generation from intermittent sources. Currently, Li-ion (150 Wh kg⁻¹) and Li-ion-polymer (180 Wh kg⁻¹) batteries^[1] are the most promising storage platforms for many applications. It is understood however that the intercalation-based cathodes used in these technologies provide limited opportunities for the sort of advancement in specific energy required to keep pace with growing demand.^[2–4] Replacing cathodes with conversion materials such as sulfur, oxygen, or carbon dioxide, removes these limitations, but introduces new challenges associated with dissolution, transport, and parasitic reactions between battery anodes and redox products in cathodes.^[2,5] Lithium–sulfur (Li–S) battery is the most studied and arguably the most promising candidate for commercial use for at least three reasons: (i) The Li–S battery offers tenfold higher energy storage capacity (specific capacity 1675 mAh g⁻¹ and theoretical energy density 2600 Wh kg⁻¹) than any of the commercial Li-ion batteries; (ii) sulfur is earth abundant and inexpensive (\$0.02 g sulfur⁻¹), leading to low-cost high-energy batteries;^[6,7] and (iii) sulfur is environmentally benign, reacts spontaneously and reversibly with lithium.^[5,8,9] Despite these benefits, Li–S cells suffer from poor cycling efficiency and short lifetimes stemming from the complex solution chemistry of lithium sulfide and lithium polysulfide (LiPS) products from the cathode.^[10–13] The most successful efforts have been devoted to cathode configurations/materials to provide physical confinement^[11,14,15] and chemical adsorption^[16–18] for LiPS to prevent its dissolution and uncontrolled redox reaction with lithium metal.

Membranes able to regulate diffusion of cathode products, without compromising ion transport between anode and cathode provide a means for controlling LiPS loss from the cathode and for preventing shuttling in the Li–S cells.^[19–31] For instance, carbon and ceramic coatings on the porous separator

using slurry/tape casting methods have been argued to provide a mechanism for blocking passage of LiPS to the anode, while providing a mechanism for electrochemical utilization and adsorption of the LiPS during the cycle.^[20–29] A persistent challenge has been how to implement these changes in a practical Li–S cell, where the mass of inactive material required for stable operation is already a serious concern.

This article reports on the fabrication of membranes by coating carbon, polymers, and inorganic particles on polyolefin separators. The conventional Langmuir–Blodgett (LB) technique has been applied in a number of fields of science and technology to form molecular-thick films with amphiphilic molecules, carbon, and inorganic particles for potential applications for thin film electronic devices.^[32–35] We have developed a new coating technique, a binder-free coating method, termed Langmuir–Blodgett–Scooping (LBS), to rapidly create multifunctional coatings. The coating process is faster than conventional LB deposition, doctor-blade coating, tape casting, and vacuum filtration methods and as such make the method promising for large-scale applications. We use the approach to create coatings of multi-walled carbon nanotube (MWCNT), polyaniline (PANI), titania nanoparticles (titania NPs), and combinations of these materials on commercial Celgard polypropylene separators with single-particle thickness resolution.^[36] PANI is an electron conducting polymer that contains amine/imine groups able to interact strongly and specifically with LiPS via electrostatic interactions. Membranes based on this material are therefore able to bind to and thereby hinder transport of LiPS between the cathode and anode of Li–S cells, and at the same time allow the adsorbed LiPS to remain electrochemically accessible during cycling.^[37] PANI was previously used in Li–S cathodes to encapsulate sulfur in yolk–shell,^[38] nanotubes,^[37] nanorods^[39] structures, and coat thin layer of PANI on S/C composites.^[40] In this work, PANI is applied directly to the separator without any additional treatment and under ambient conditions. There are a variety of coating methods suitable for materials of specific geometries with most methods requiring use of a binder material for cohesion. The coating method developed in the present work takes advantage of Marangoni stresses and self-assembly at the air/water interface to create highly organized monolayer on non-reactive substrates. Application of these approaches for fabricating MWCNT, PANI, and titania NPs in a layer-by-layer, laminated format provides strategies for creating membranes with low material content and in a porous 3D network morphology able to suppress loss of LiPS, while simultaneously maintaining electrochemical access to the material.^[41] The laminated PANI structure used in the study is comprised of ≈80 nm thick MWCNT adhesion layer for PANI, followed by ≈6 μm thick PANI, ≈900 nm thick titania NP, and ≈3 μm thick PANI (overall thickness of ≈10 μm) with total

M. S. Kim, S. Choudhury, Prof. L. A. Archer
Department of Chemical and Biomolecular Engineering
Cornell University
Ithaca, NY 14853-5201, USA
E-mail: laa25@cornell.edu

M. S. Kim
Korea Institute of Science and Technology
Hwarangno 14-gil 5, Seongbuk-gu, Seoul 02792, Republic of Korea
Dr. L. Ma
Department of Materials Science
Cornell University
Ithaca, NY 14853-5201, USA



DOI: 10.1002/admi.201600450

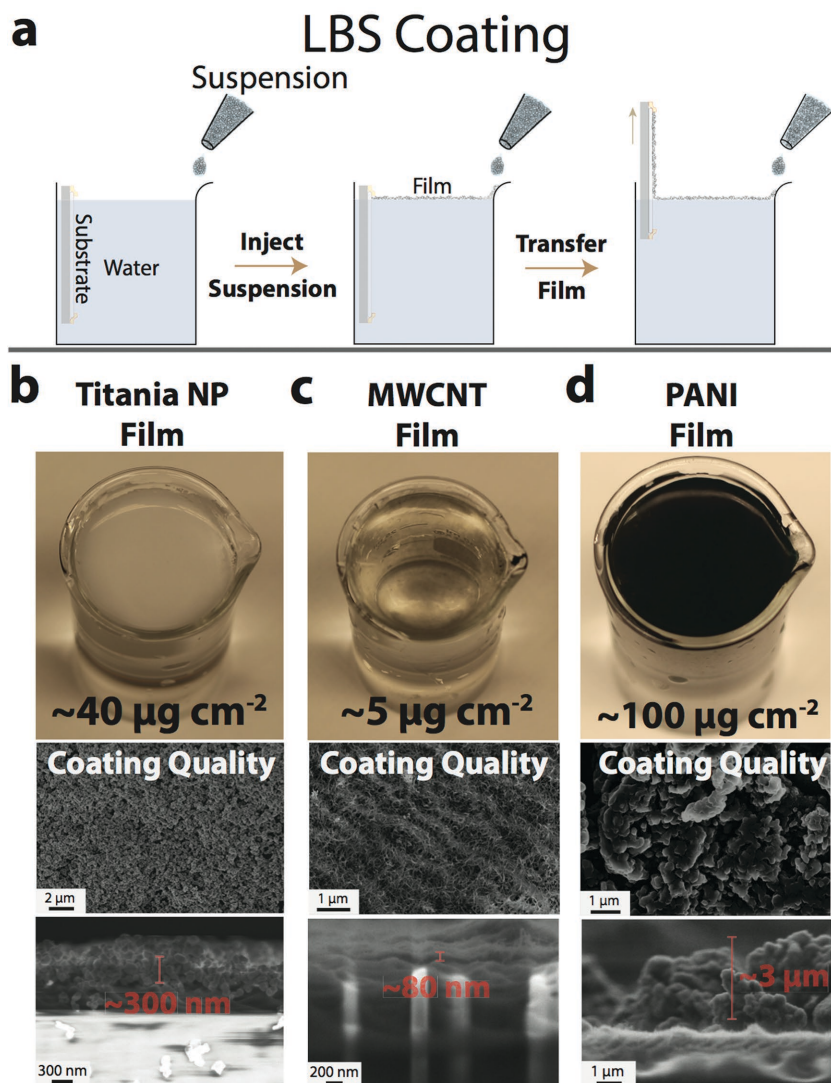


Figure 1. a) Schematic illustration of the LBS coating process. Physical images of self-assembled films of various materials at the air–water interface for different gravimetric compositions and chemistry: b) Titania NP, c) MWCNT, and d) PANI. The SEM images show the high quality of the various coatings and the film thicknesses achieved per material coating layer on Celgard separators.

material loading of $\approx 400 \mu\text{g cm}^{-2}$. When used in Li–S batteries with low and high material loadings, we show that the prepared membranes lead to high reversible capacities (1220, 1150, and 1000 mAh g^{-1} at 0.5, 1, and 2 C, respectively), with stable and high Coulombic efficiencies ($\approx 97\%$ at the 100th cycle), without the need for common LiNO_3 additives in the electrolyte.

Figure 1a illustrates the LBS method. The approach utilizes self-assembly of particles to form a well-packed film (Videos, Supporting Information). The self-assembly is induced by spreading and mixing of water miscible solvent at the surface of water^[42] and surface tension gradients.^[43] Briefly, a volatile and water miscible solvent is injected at the air–water interface, induces strong flows at the surface that drive the spreading of the solvent by the combined effect of surface tension gradient from the two different fluids, known as Marangoni effect.^[44] The spreading pressure leads to rapid and highly ordered

assembly of structures present at the air–water interface, which can be transferred to any non-reactive substrates by immersion and removal of the substrate from the liquid. Because of its speed ($<10 \text{ sec}$), the method can be applied repeatedly to create multilayer ordered coatings of a variety of materials in layer-by-layer format. For the coating process, only ethanol with nanopowders and water are required. Figure 1b shows a self-assembled film of titania NPs with gravimetric density of $\approx 40 \mu\text{g cm}^{-2}$ and thickness of $\approx 300 \text{ nm}$ created using the approach. Figure 1c,d illustrates analogous results for coating of MWCNT and PANI with gravimetric density and thickness of $\approx 5 \mu\text{g cm}^{-2}$, $\approx 80 \text{ nm}$ and $\approx 100 \mu\text{g cm}^{-2}$, $\approx 3 \mu\text{m}$, respectively. In all cases, it is apparent that the obtained coatings are of high quality, with particles well packed/ordered and uniformly distributed throughout the materials, with no evidence of defects.

To understand the fundamental processes responsible for self-assembled titania NP, MWCNT, and PANI films, surface pressure profiles of the three materials were measured using a conventional Langmuir–Blodgett trough (LBT) as shown in **Figure 2**. To facilitate comparisons, profiles obtained using LBS and LBT are compared, and three surface pressures are chosen for each material coincident with the overly packed, fully packed, and poorly packed states. The full spectrum of surface film packing densities are apparent from the LBT profiles, including a regime of film buckling and folding at high surface pressures (see **Figure S1**, Supporting Information). The onset of folding behavior is evident as an inflection point where the concavity of the profile curve changes, which provide a convenient means of assessing achievement of fully packed high-quality films.

Figure 2a shows the surface pressure profiles of titania NP using LBT and LBS methods. Three surface pressures are chosen ($A = 54 \text{ mN m}^{-1}$, $B = 28 \text{ mN m}^{-1}$, $C = 1 \text{ mN m}^{-1}$) to observe the titania NP coatings on the separator. A, B, and C represent the surface pressures where the nanoparticles are overly packed, fully packed, and poorly packed, respectively. Analysis of the scanning electron microscopy (SEM) images for titania NP coated separators, highest coating quality is made at point B. This means that around surface pressure of 28 mN m^{-1} , which is around the inflection point at 31 mN m^{-1} , will yield highly packed particle film on the water surface. The information is then used to verify the coating quality of LBS method. For the self-assembled films using LBS method, we have measured the surface pressure profiles of the resulting films. In **Figure 2a**, LBS surface pressure profile starts at a surface pressure of 28 mN m^{-1} , and no inflection point is observed. The starting

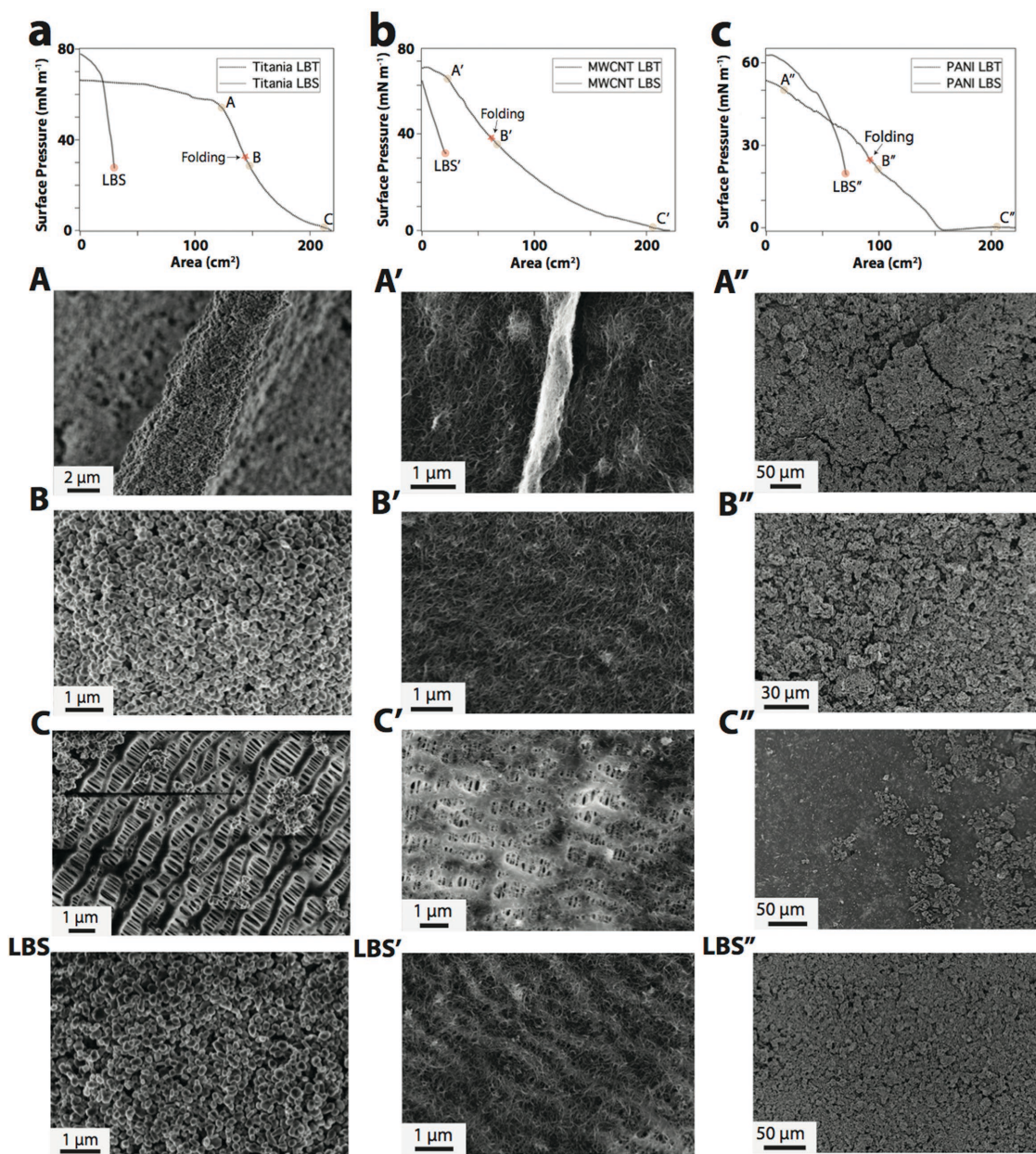


Figure 2. Surface pressure profiles for conventional LBT and LBS coatings of various material chemistries with the corresponding SEM images obtained at designated surface pressures to illustrate the coating quality achieved. a) Titania NP ($A = 54 \text{ mN m}^{-1}$, $B = 28 \text{ mN m}^{-1}$, $C = 1 \text{ mN m}^{-1}$, $LBS = 28 \text{ mN m}^{-1}$, $Folding = 31 \text{ mN m}^{-1}$); b) MWCNT ($A' = 63 \text{ mN m}^{-1}$, $B' = 35 \text{ mN m}^{-1}$, $C' = 2 \text{ mN m}^{-1}$, $LBS' = 32 \text{ mN m}^{-1}$, $Folding = 37 \text{ mN m}^{-1}$); and c) PANI ($A'' = 50 \text{ mN m}^{-1}$, $B'' = 21 \text{ mN m}^{-1}$, $C'' = 3 \text{ mN m}^{-1}$, $LBS'' = 20 \text{ mN m}^{-1}$, $Folding = 24 \text{ mN m}^{-1}$).

surface pressure indicates that the self-assembly process exerts the pressure of 28 mN m^{-1} , and absence of the inflection point in the LBS profile verifies that the LBS method starts at highly packed state. Hence, the uniform titania NP coating on the separator is made as shown in Figure 2a SEM at LBS that matches well with the coating at point B. Analogous measurements for MWCNT (Figure 2b) and PANI (Figure 2c) were used to assess the state of order in these films. The surface pressures of $A' = 63 \text{ mN m}^{-1}$, $B' = 35 \text{ mN m}^{-1}$, $C' = 2 \text{ mN m}^{-1}$ for MWCNT and $A'' = 50 \text{ mN m}^{-1}$, $B'' = 21 \text{ mN m}^{-1}$, $C'' = 3 \text{ mN m}^{-1}$ for PANI are chosen to investigate the film qualities. Highest coating

qualities are obtained for B' and B'' for MWCNT and PANI. The folding point for MWCNT and PANI are 37 and 24 mN m^{-1} , and around these surface pressures yield optimized coating films. As a result, LBS coating of MWCNT and PANI at LBS' (32 mN m^{-1}) and LBS'' (20 mN m^{-1}) yield high qualities as we see in Figure 2b,c.

Building upon these fundamental studies, we employed the LBS method to create membranes in which the titania NP layers are sandwiched by PANI layers (see Figure 3a) adhered to Celgard by thin MWCNT layer. As discussed earlier, this design was motivated by the hypothesis that a flexible

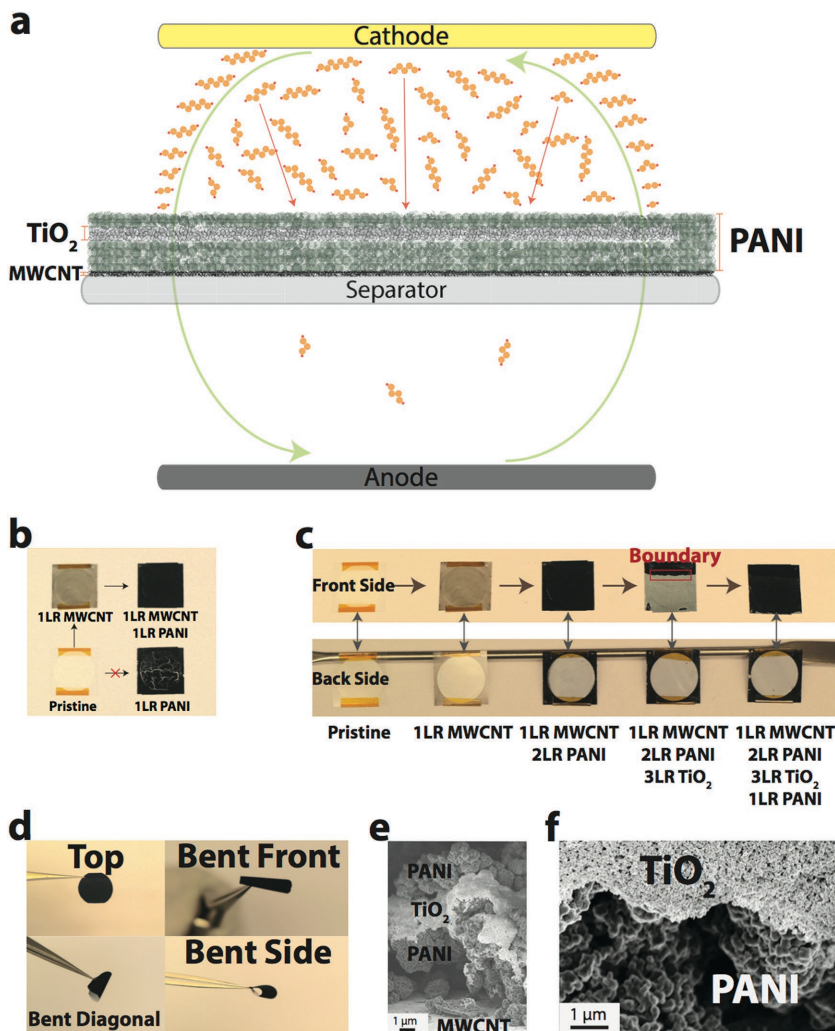


Figure 3. a) Schematic of laminated separator coating structure illustrating LiPS flux diagram during the charge/discharge of the Li-S cell. b) Demonstration of thin layer coatings of MWCNT as an effective adhesion layer for PANI coating. c) Demonstration of single-sided LBS coatings and the layer-by-layer coating process to fabricate the laminated PANI separator. d) Illustration of the bendability and toughness of the as-prepared laminated PANI separator membranes. e) Cross-sectional SEM image of laminated PANI separator. f) SEM image of titania NP-PANI boundary (three coating layers of titania NP on top of PANI, see the red box in (c)).

membrane in a clip-like configuration in which two electronically conductive layers bracket sorbent NP layer would facilitate efficient trapping of LiPS in the membrane and utilization of the trapped LiPS by the conductive layers for high active material utilization. Figure 3c shows the layer-by-layer configuration of the coatings. As illustrated in Figure 3d and Figure S2 (Supporting Information) the membranes are mechanically strong and their structure is completely preserved after mechanical distortion. Figure 3e shows the cross-sectional image of laminated PANI structure which is $\approx 10 \mu\text{m}$ thick. To observe the boundary region that is indicated with the red box in Figure 3c, we imaged this region using SEM. It is apparent that a very compact and porous 3D titania NP network is present on the top of PANI coatings.

To investigate the effectiveness of the resultant membranes in regulating LiPS transport and utilization in Li-S cells,

membranes based on the individual components with 1–5 layers ($\approx 3\text{--}15 \mu\text{m}$ thick) were studied as separators in Li-S cells and the results compared with those based on the laminated MWCNT-PANI/titania/PANI design. Figure S3 (Supporting Information) reports the cycling performance of the Li-S cells with one, three, and five coating layers of PANI alone on the separator, with 1 M LiTFSI in a 1:1 DME/DOL solvent mixture with no LiNO_3 as electrolyte, polyethyleneimine-MWCNT-sulfur composite cathode (PEISC),^[18] and Li metal anode. It is apparent in Figure S3 (Supporting Information) that improved capacity retention and higher Coulombic efficiency (CE) are achieved as the number of PANI coatings increases on the separator. For the 5LR PANI separator, a capacity of $\approx 1000 \text{ mAh g}^{-1}$ and 96% CE are achieved at the 100th cycle for a fixed 0.5 C discharge/charge rate. This can be compared to the results for the uncoated/pristine separator, which exhibits a capacity of 430 mAh g^{-1} and CE of 80% after the 100th cycle at 0.5 C. The voltage profiles of 5LR PANI separator are shown in Figure S3 (Supporting Information). Figure S4 (Supporting Information) provides a more comprehensive account of the electrochemical cycling behaviors of the Li-S cells with 5LR PANI separator where results at three different C-rates: 0.5, 1, and 2 C are reported. At the 100th cycle, capacities of ≈ 1000 , ≈ 860 , and $\approx 740 \text{ mAh g}^{-1}$, and $\approx 97\%$ CE are obtained for 0.5, 1, and 2 C, respectively. The voltage profiles of 5LR PANI at three different C-rates are shown in Figure S4 (Supporting Information). For comparison, Figure S5 (Supporting Information) shows the cycling performance of Li-S cells with 5LR PANI separator at 0.5, 1, and 2 C when 0.05 M LiNO_3 is added in the electrolyte. Li-S cells with the 5LR PANI on the separator achieved $\approx 99.9\%$ CE for 100th

cycles with the small amount of LiNO_3 in the electrolyte. The control's CE, however, remained $\approx 91\%$ in the presence of small amount of LiNO_3 due to more severe shuttling effect compared to that of the modified separator cells. The capacity retention, on the other hand, increased in the control due to the large number of amine groups in PEI chains, which anchor LiPS in the cathode.^[18] With the 5LR PANI coated separator at 100th cycle, capacities of ≈ 1000 , ≈ 900 , and $\approx 830 \text{ mAh g}^{-1}$, and $\approx 99.9\%$ CE are obtained for 0.5, 1, and 2 C, respectively. The voltage profiles of 5LR PANI at three different C-rates are shown in Figure S5 (Supporting Information).

Next, we consider Li-S cells based on the laminated membrane composed of $\approx 80 \text{ nm}$ thick (1LR) MWCNT, $\approx 9 \mu\text{m}$ thick (3LR) PANI, and $\approx 900 \text{ nm}$ thick (3LR) titania NP on Celgard. In comparison to the single-component 5LR PANI (thickness of $\approx 15 \mu\text{m}$ and mass loading of $\approx 500 \mu\text{g cm}^{-2}$) based membranes

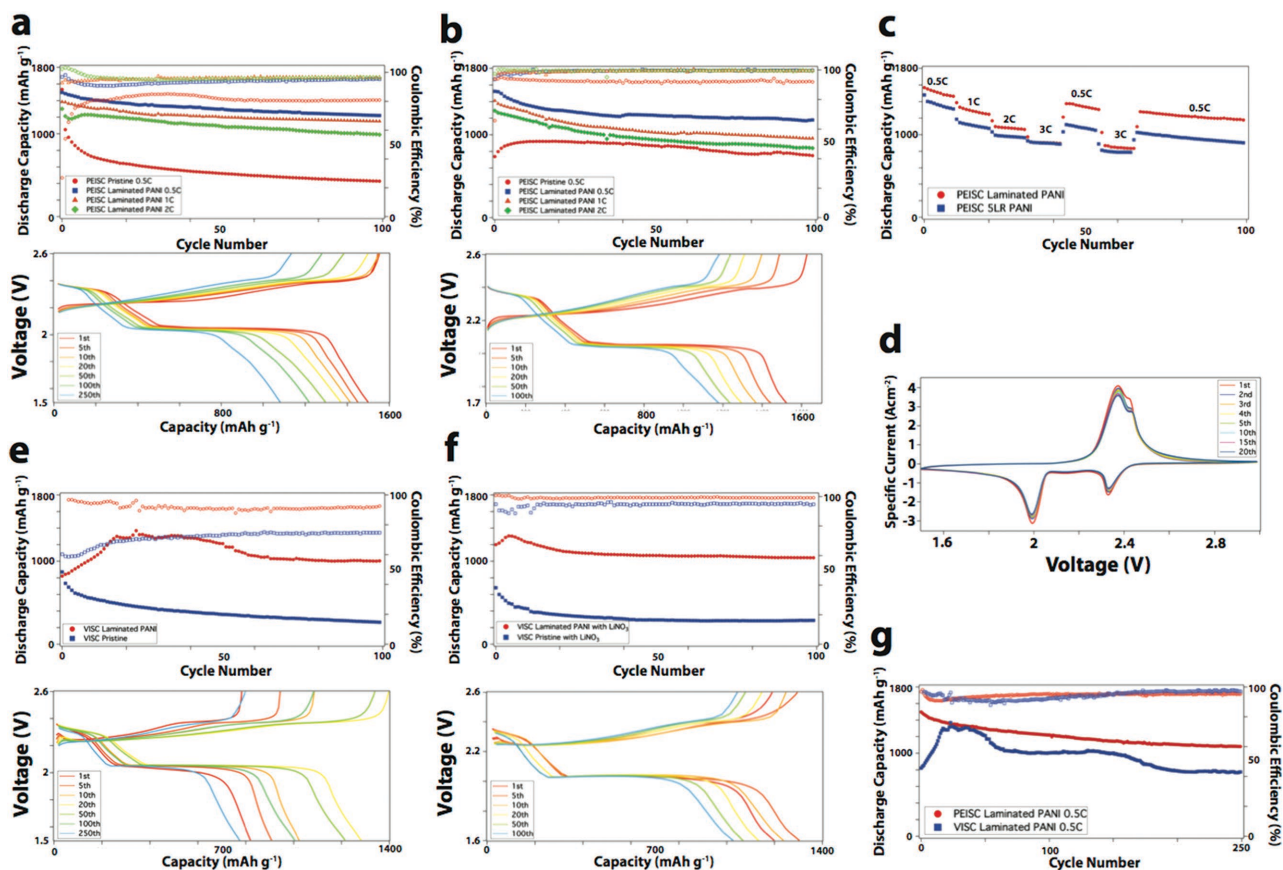


Figure 4. a) Galvanostatic discharge capacity and Columbic efficiency versus cycle number at various C-rates and voltage profiles for a fixed rate of 0.5 C for Li-S cells based on laminated PANI and pristine Celgard separators and employing PEISC. Notably, no LiNO₃ additives were used in the electrolyte of these cells. b) Galvanostatic discharge capacity and Columbic efficiency versus cycle number at various C-rates and voltage profiles for a fixed rate of 0.5 C for Li-S cells based on laminated PANI and pristine Celgard separators and employing PEISC with 0.05 M LiNO₃ in the electrolyte. c) Cycling performance at various C-rates for Li-S cells based on PEISC cathodes, laminated PANI separator, and 5LR PANI coated separator. For these measurements, no LiNO₃ additive was used in the electrolyte. d) Cyclic voltammogram of Li-S cells based on PEISC and, laminated PANI separators with no LiNO₃ additive in the electrolyte. e) Cycling performance of the laminated PANI and pristine Celgard separators in Li-S cells based on a VISC and LiNO₃-free electrolyte at 0.5 C. f) Cycling performance of the laminated PANI separator and pristine separator with VISC and 0.05 M LiNO₃ in the electrolyte Li-S cells for 100 cycles at 0.5 C and the voltage profiles of the laminated PANI separator with VISC at 0.5 C for various cycles. g) Long time cycling characteristics of Li-S cells at 0.5 C based on PEISC and VISC, laminated PANI separators, and LiNO₃-free electrolyte.

assessed in the last section, the laminated PANI coating though more complex is thinner ($\approx 10 \mu\text{m}$) and introduces a lower material mass ($\approx 400 \mu\text{g cm}^{-2}$) to the Li-S cell. **Figure 4a** reports cycling performance and voltage profiles for Li-S cells based on these laminated membranes. It is seen that capacities of 1220, 1150, and 1000 mAh g⁻¹ are obtained at 0.5, 1, and 2 C, respectively, with $\approx 97\%$ CE at 100th cycle. Comparison with the results from the uncoated membranes shows that the capacity has approximately doubled and the CE increased markedly. It is instructive to compare these results with analogous ones reported for other materials configurations, e.g., cation-shield (CE $\approx 95\%$)^[30] and ionomer film (CE $\approx 97\%$)^[31] reported previously for regulating LiPS mass transport and shuttling in Li-S cells. It is apparent that the CE values achieved for the laminated PANI membranes are comparable with those reported for single ion conductors. A small amount of LiNO₃ (0.05 M) was added in the electrolyte to observe its effect on electrochemical performance of Li-S cells with laminated membranes. As expected, CE values approaching $\approx 99.9\%$ are achieved without affecting cell

capacity and cycling stability (Figure 4b). Voltage profiles of the laminated PANI separator Li-S cells at three different C-rates with/without LiNO₃ in the electrolyte are shown in Figure S6 (Supporting Information). Moreover, various C-rate performance is measured with the laminated PANI separator with no LiNO₃ in the electrolyte (see Figure 4c). As the C-rates increase (0.5 to 1, 1 to 2, and 2 to 3 C), 14%, 15%, and 17% decrease in the capacity are observed with the recovery capacity of 1310 mAh g⁻¹, which is 10% decrease from the previous 0.5 C cycling, after cycling the cell from 0.5 to 3 C for ten cycles at each C-rate. Comparing this result with the Li-S cell with 5LR PANI separator, higher recovery capacity is obtained (Laminated PANI: 1310 mAh g⁻¹ and 5LR PANI: 1110 mAh g⁻¹) for the laminated PANI without losing the high C-rate performances even though lesser amount of PANI is used. Together, these results provide strong support for our hypothesis that membranes based on laminated PANI structures simultaneously provide a path toward high-energy and high-power Li-S cells by regulating transport of LiPS without compromising active material utilization in the cathode.

Figure 4d reports cyclic voltammograms of the Li–S cell with laminated PANI separator for LiNO₃ free system. Scan rate of 0.1 mV s⁻¹ and voltage window of 1.5–3V are used to perform the measurement. The cathodic scans show distinctive voltage plateaus at 2.3 and 2 V. The first peak at 2.3 V represents cyclic sulfur breaking and forming high-order LiPS ions whereas the next peak at 2 V represents the reduction of high-order LiPS ion to low-order LiPS. These voltage plateaus are typical for Li–S cells that represent two-step reduction process of elemental sulfur in cyclic form. For the anodic scans, the distinctive voltage plateaus and oxidation peaks, are observed at 2.37 and 2.43 V based on the phase transition mechanism.^[10] Stable anodic and cathodic peak positions are achieved for several cycles. Hence, highly reversible electrochemical reactions are confirmed for the Li–S cell with laminated PANI separator without LiNO₃ in the electrolyte.

A disadvantage of the PEISC is relatively low sulfur loading (1.2 mg cm⁻² S and content of 50% S). State-of-the-art Li–S cells require substantially higher sulfur loadings and content in the cathode. As more rigorous tests of the laminated PANI membranes, we also assessed the materials, vapor infused sulfur cathode (VISC), in Li–S cells with higher sulfur loading (3.5 mg cm⁻² S and 68% S), created by a previously reported vapor infusion method.^[11] Figure 4e reports cycling performance and voltage profiles of Li–S cells with both the pristine and laminated PANI separator membranes, with VISC and no LiNO₃ in the electrolyte. The control Li–S cell exhibits a capacity of ≈270 mAh g⁻¹ and 74% CE after 100 cycles at 0.5 C. In contrast the laminated PANI separator displays a capacity of ≈1000 mAh g⁻¹ and 94% CE after the 100 cycle at 0.5 C. Closer inspection of the cycling results for the VISC using the laminated PANI membrane separator shows initial increase in the discharge capacity. This behavior is understood to be a manifestation of the laminated coatings capacity to reutilize LiPS as it is built up in the sorbent layer in the membrane.^[45] Our results therefore verify that the laminated PANI membrane separator is capable of cycling high sulfur loading cathodes in cells without LiNO₃ in the electrolyte. As before, we also performed studies in which 0.05 M LiNO₃ is used in the electrolyte (see Figure 4f). The results show that while similar capacity is observed as for the LiNO₃ free case, ≈99.9% CE is achieved. Figure 4e,f reports voltage profiles for the VISC cells with and without LiNO₃ in the electrolyte, it is apparent that they are stable in both cases. Figure 4g shows that these favorable results are preserved in long-term cycling experiments, where Li–S cells with PEISC and VISC and no LiNO₃ are observed to yield discharge capacities of 1090 mAh g⁻¹ and 96% CE (PEISC) and 780 mAh g⁻¹ and 97% CE (VISC) after the 250 discharge cycle at 0.5 C. We therefore conclude that membranes based on the proposed laminated PANI configuration using existing Celgard separator as a substrate provide a promising path toward Li–S cells with stable electrochemical performance. The results also show that compact layers of PANI and titania NPs created by LBS work synergistically to improve membrane performance.

The cycled laminated PANI membranes were investigated via SEM and energy-dispersive X-ray spectroscopy (EDXS). Figure S7 (Supporting Information) shows cross-sectional and top view SEM and elemental mapping of sulfur, nitrogen, titanium, and carbon on the laminated PANI separator that is

cycled 100 times with VISC and no LiNO₃ in the electrolyte. The laminated structure is observed to be well maintained after complete 100 cycles. This is due to the property of the PANI, which is known as soft polymer that could withstand the pressures from volumetric expansion of sulfur during the charge–discharge process.^[37] A strong field map of sulfur is also apparent in the cross-sectional and top view of the laminated PANI-based membranes.

Figure 5a shows the AC impedance (ACI) of Li–S cells with pristine and the laminated PANI separators with VISC and no LiNO₃ in the electrolyte before and after cycling. The upper ACI data show the impedance comparison between the Li–S cells with the laminated PANI and pristine separator before cycling, and lower impedance is measured for the laminated PANI separator Li–S cell indicating that the high conductivity of PANI helps to reduce the interfacial impedance. The bottom ACI data show the impedance data of the laminated PANI separator Li–S cell before and after 100th cycle. Slight increase of impedance is observed after 100th discharge. This is because the laminated PANI coatings adsorb LiPS which increases the interfacial impedance. After 100th charge, the impedance gets lower than that of 100th discharge but higher than that of initial. This is due to the adsorbed LiPS is reutilized during the charge process which lowers the interfacial impedance, and since sulfur is present on the surface of the coatings on the separator, higher impedance is measured compared to the initial impedance measurement which the surfaces are free from LiPS and sulfur. Hence, reutilization and lower impedance of adsorbed LiPS are observed with the laminated PANI separator. We have also performed self-discharge experiment with the laminated PANI separator Li–S cells with VISC and no LiNO₃ in the electrolyte (see Figure 5b). With the laminated PANI separator, the Li–S cell can stably remain as initial state >200 h whereas the Li–S cell with the pristine separator fails after 20 h. This indicates that the top surface of PANI on the cathode provides a protection layer to alleviate the self-discharge and active material loss during shelf time.

We have compared our results with current literature values as shown in Figure 5c. It is apparent that the Li–S cell performances achieved with the proposed membranes stand out among current literature works in terms of the capacity and high rate performances achievable for high sulfur loadings in the cathode.^[11,15,18,20,21,23,29,30,46–51] The effect of the membranes is seen to be more dramatic at high current rates—at 2 C, for example, the results obtained using the laminated membrane separators are superior to all other literature reports at comparable sulfur loading. The gravimetric and areal capacities of the laminated PANI separator for PEISC and VISC are ≈1050 mAh g⁻¹, 1.2 mAh cm⁻² and ≈1000 mAh g⁻¹, 3.5 mAh cm⁻², respectively.

In this study, we report a facile coating methodology termed LBS that takes advantage of self-assembly and Marangoni stresses at an air/water interface to rapidly create multifunctional coatings of PANI, titania NPs, MWCNT, and combinations of these materials on porous and non-porous solid supports. More generally, the LBS method is used to create nanoparticle and polymer coatings with single-particle/molecule thickness resolution on any non-reactive substrate, without the need for binders. The LBS technique also holds for large-scale industrial deployment since the method can be implemented in any vessel (i.e., no Langmuir trough, floats, or baffles are needed) using physical forces alone to create ordered

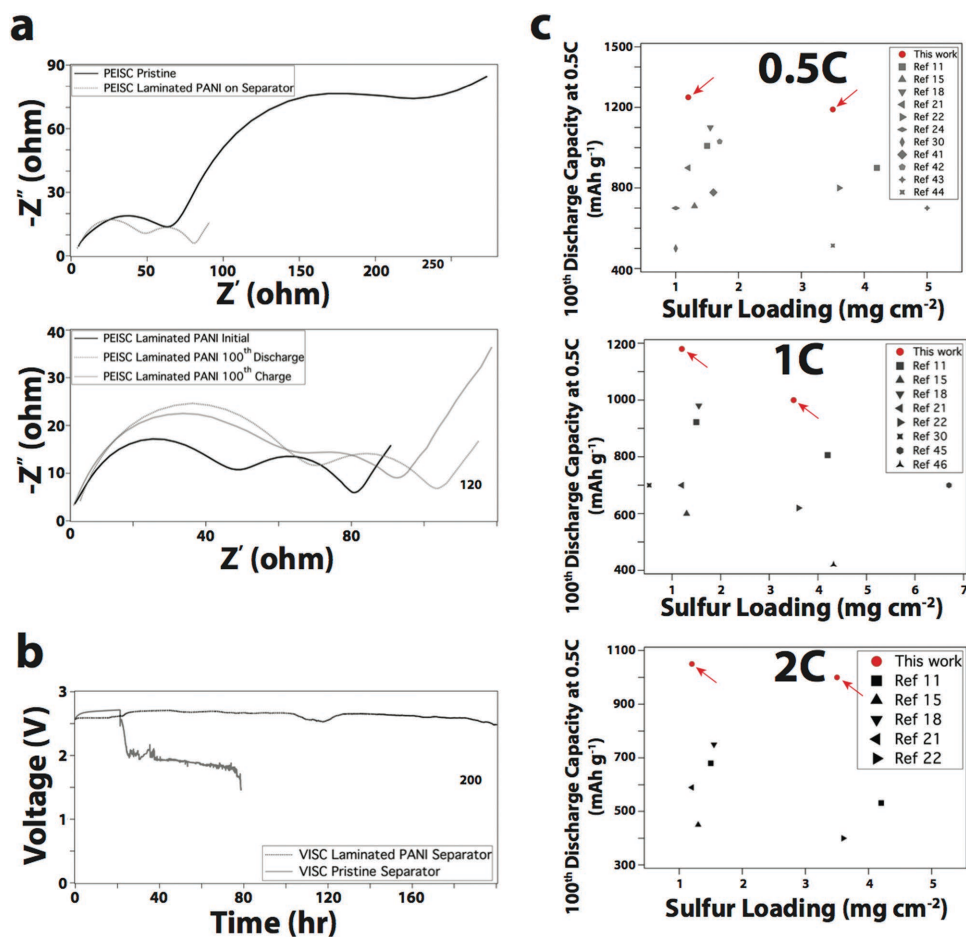


Figure 5. a) AC impedance spectra of Li-S cells based on PEISC and laminated PANI separator prior to (upper plot) and after (lower plot) 100 cycles. No LiNO_3 was used in the electrolyte. b) Self-discharge characteristics of Li-S cells based on VISC and pristine/laminated PANI separators with no LiNO_3 in the electrolyte. c) Comparison of discharge capacity for Li-S cells obtained at three different C-rates and after 100 cycles from our work and other studies reported in the literature.^[11,15,18,20,21,23,29,30,46-51]

nanoparticle films and takes advantage of benign chemicals for the coating process. Sequential applications of the approach allow us to fabricate thin, multifunctional MWCNT-PANI/titania/PANI coatings in layer-by-layer configuration on polyolefin separators used for Li-S batteries. Application of the resultant membranes (separator+multifunctional coatings) to Li-S batteries is shown to enable cells with high capacity and stable cycling over a range of discharge rates (≈ 1220 , ≈ 1150 , and $\approx 1000 \text{ mAh g}^{-1}$ are obtained at 0.5, 1, and 2 C respectively, with $\approx 97\%$ CE at 100th cycle), without the need for LiNO_3 additives in the electrolyte.

Supporting Information

Supporting Information is available from the Wiley Online Library or from the author.

Acknowledgements

M.S.K. and L.M. contributed equally to this work. The authors acknowledge support of the National Science Foundation Partnerships

for Innovation Program (Grant No. IIP-1237622). Electron microscopy, X-ray diffractometry, X-ray spectroscopy facilities, and optical spectrometers available through the Cornell Center for Materials Research (CCMR) were used for this work (NSF Grant No. DMR-1120296). M.S.K. acknowledges partial support from the Korea Institute of Science and Technology (KIST) Institutional Program.

Received: May 17, 2016

Revised: June 16, 2016

Published online:

- [1] T. J. Miller, *Electrical Energy Storage for Vehicles: Targets and Matrics* **2009**, p. 1, U.S. Department of Energy's Advanced Research Projects Agency - Energy, USA.
- [2] M. Armand, J.-M. Tarascon, *Nature* **2008**, *451*, 652.
- [3] J. B. Goodenough, Y. Kim, *Chem. Mater.* **2010**, *22*, 587.
- [4] C.-X. Zu, H. Li, *Energy Environ. Sci.* **2011**, *4*, 2614.
- [5] P. G. Bruce, S. A. Freunberger, L. J. Hardwick, J.-M. Tarascon, *Nat. Mater.* **2011**, *11*, 172.
- [6] J. Hassoun, B. Scrosati, *Adv. Mater.* **2010**, *22*, 5198.
- [7] Z. Yang, J. Guo, S. K. Das, Y. Yu, Z. Zhou, H. D. Abruna, L. A. Archer, *J. Mater. Chem. A* **2013**, *1*, 1433.

- [8] Y. G. Guo, J. S. Hu, L. J. Wan, *Adv. Mater.* **2008**, *20*, 2878.
- [9] L. Ma, K. E. Hendrickson, S. Wei, L. A. Archer, *Nano Today* **2015**, *10*, 315.
- [10] Y. V. Mikhaylik, J. R. Akridge, *J. Electrochem. Soc.* **2004**, *151*, A1969.
- [11] N. Jayaprakash, J. Shen, S. S. Moganty, A. Corona, L. A. Archer, *Angew. Chem.* **2011**, *50*, 5904.
- [12] J. Nelson, S. Misra, Y. Yang, A. Jackson, Y. Liu, H. Wang, H. Dai, J. C. Andrews, Y. Cui, M. F. Toney, *J. Am. Chem. Soc.* **2012**, *134*, 6337.
- [13] Z. W. Seh, W. Li, J. J. Cha, G. Zheng, Y. Yang, M. T. McDowell, P.-C. Hsu, Y. Cui, *Nat. Commun.* **2013**, *4*, 1331.
- [14] X. Ji, K. T. Lee, L. F. Nazar, *Nat. Mater.* **2009**, *8*, 500.
- [15] H. Wang, Y. Yang, Y. Liang, J. T. Robinson, Y. Li, A. Jackson, Y. Cui, H. Dai, *Nano Lett.* **2011**, *11*, 2644.
- [16] L. Ma, S. Wei, H. L. Zhuang, K. E. Hendrickson, R. G. Hennig, L. A. Archer, *J. Mater. Chem. A* **2015**, *3*, 19857.
- [17] L. Ma, H. Zhuang, Y. Lu, S. S. Moganty, R. G. Hennig, L. A. Archer, *Adv. Energy Mater.* **2014**, *4*, 390.
- [18] L. Ma, H. L. Zhuang, S. Wei, K. E. Hendrickson, M. S. Kim, G. Cohn, R. G. Hennig, L. A. Archer, *ACS Nano* **2015**, *10*, 1050.
- [19] K. E. Hendrickson, L. Ma, G. Cohn, Y. Lu, L. A. Archer, *Adv. Sci.* **2015**, *2*, 68.
- [20] H. Bin Yao, K. Yan, W. Li, G. Zheng, D. Kong, Z. W. Seh, V. K. Narasimhan, Z. Liang, Y. Cui, *Energy Environ. Sci.* **2014**, *7*, 3381.
- [21] J. Balach, T. Jaumann, M. Klose, S. Oswald, J. Eckert, L. Giebeler, *Adv. Funct. Mater.* **2015**, *25*, 5285.
- [22] G. Wang, Y. Lai, Z. Zhang, J. Li, Z. Zhang, *J. Mater. Chem. A* **2015**, *3*, 7139.
- [23] Z. Zhang, Y. Lai, Z. Zhang, J. Li, *Solid State Ionics* **2015**, *278*, 166.
- [24] H. Wei, B. Li, Y. Zuo, D. Xia, *ACS Appl. Mater. Interfaces* **2014**, *6*, 20276.
- [25] F. Li, G. Zhou, S. Pei, L. Li, D. W. Wang, S. Wang, K. Huang, L. C. Yin, H. M. Cheng, *Adv. Mater.* **2014**, *26*, 625.
- [26] Z. Xiao, Z. Yang, L. Wang, H. Nie, M. Zhong, Q. Lai, X. Xu, L. Zhang, S. Huang, *Adv. Mater.* **2015**, *27*, 2891.
- [27] Z. Zhang, Y. Lai, Z. Zhang, K. Zhang, J. Li, *Electrochim. Acta* **2014**, *129*, 55.
- [28] Y. Chen, N. Liu, H. Shao, W. Wang, M. Gao, C. Li, H. Zhang, A. Wang, Y. Huang, *J. Mater. Chem. A* **2015**, *3*, 15235.
- [29] Z. Zhang, Z. Zhang, J. Li, Y. Lai, *J. Solid State Electrochem.* **2015**, *19*, 1709.
- [30] J.-Q. Huang, Q. Zhang, H.-J. Peng, X.-Y. Liu, W.-Z. Qian, F. Wei, *Energy Environ. Sci.* **2014**, *7*, 347.
- [31] Z. Jin, K. Xie, X. Hong, Z. Hu, X. Liu, *J. Power Sources* **2012**, *218*, 163.
- [32] X. Chen, S. Lenhert, M. Hirtz, N. a. N. Lu, H. Fuchs, *Acc. Chem. Res.* **2007**, *40*, 393.
- [33] X. Li, G. Zhang, X. Bai, X. Sun, X. Wang, E. Wang, H. Dai, *Nat. Nanotechnol.* **2008**, *3*, 538.
- [34] Y. Lu, Y. Yang, A. Sellinger, M. Lu, J. Huang, H. Fan, R. Haddad, G. Lopez, A. R. Burns, D. Y. Sasaki, J. Shelnut, C. J. Brinker, *Nature* **2001**, *410*, 913.
- [35] Q. Cao, S. Han, G. S. Tulevski, Y. Zhu, D. D. Lu, W. Haensch, *Nat. Nanotechnol.* **2013**, *8*, 180.
- [36] M. S. Kim, L. Ma, S. Choudhury, S. S. Moganty, S. Wei, L. A. Archer, *ArXiv* **2016**, preprint ArXiv: 1604.04241.
- [37] L. Xiao, Y. Cao, J. Xiao, B. Schwenzer, M. H. Engelhard, L. V. Saraf, Z. Nie, G. J. Exarhos, J. Liu, *Adv. Mater.* **2012**, *24*, 1176.
- [38] W. Zhou, Y. Yu, H. Chen, F. J. Disalvo, H. D. Abruna, *J. Am. Chem. Soc.* **2013**, *135*, 16736.
- [39] W. Li, Z. Zhang, W. Kang, Y. Tang, C.-S. Lee, *ChemElectroChem* **2016**, *3*, 1.
- [40] G. C. Li, G. R. Li, S. H. Ye, X. P. Gao, *Adv. Energy Mater.* **2012**, *2*, 1238.
- [41] S. Evers, T. Yim, L. F. Nazar, *J. Phys. Chem. C* **2012**, *116*, 19653.
- [42] H.-L. Nie, X. Dou, Z. Tang, H. D. Jang, J. Huang, *J. Am. Chem. Soc.* **2015**, *137*, 10683.
- [43] X. Fanton, A. M. Cazabat, *Langmuir* **1998**, *14*, 2554.
- [44] C. V. Sternling, L. E. Scriven, *AIChE J.* **1959**, *5*, 514.
- [45] C. H. Chang, S. H. Chung, A. Manthiram, *Small* **2016**, *12*, 174.
- [46] Y. L. Ding, P. Kopold, K. Hahn, P. A. van Aken, J. Maier, Y. Yu, *Adv. Funct. Mater.* **2015**, *26*, 1112.
- [47] Z. Li, J. T. Zhang, Y. M. Chen, J. Li, X. W. (David) Lou, *Nat. Commun.* **2015**, *6*, 8850.
- [48] T. Xu, J. Song, M. L. Gordin, H. Sohn, Z. Yu, S. Chen, D. Wang, *ACS Appl. Mater. Interfaces* **2013**, *5*, 11355.
- [49] Q. Pang, D. Kundu, L. F. Nazar, *Mater. Horiz.* **2016**, *3*, 130.
- [50] S. Chung, A. Manthiram, *Phys. Chem. Lett.* **2014**, *5*, 1987.
- [51] B. Papandrea, X. Xu, Y. Xu, C.-Y. Chen, Z. Lin, G. Wang, Y. Luo, M. Liu, Y. Huang, L. Mai, X. Duan, *Nano Res.* **2016**, *9*, 240.